A Mechanics-Based Finite Element for the Analysis of Shear-Critical Slender Reinforced Beams and Columns

Edvard P. G. Bruun, P.Eng., S.M.ASCE[1]; and Evan C. Bentz, P.Eng.[2]

Abstract: This paper presents the derivation and validation of a mechanics-based finite element for the analysis of shear-critical slender reinforced concrete beams and columns. The element can capture the load-deformation behavior associated with axial loads, bending moments, and shear in uncracked or cracked reinforced concrete using only a small number of degrees of freedom and easily measurable input parameters: the gross cross-section dimensions and steel and concrete material stress/strain curves. The element is specifically derived to represent the full reinforced concrete cross section (i.e., one element is required over the depth of a member) and consists of four nodes, with two translational degrees of freedom (DOFs) per node. This formulation facilitates modeling the interface regions between walls or joint regions, beams, or columns and lowers the numerical complexity and number of decisions that the user must make. The element shows improvements to results from design codes when validated against experimental results for 782 beams without shear reinforcement and 167 beams with shear reinforcement taken from the literature. By reducing the number of degrees of freedom, the element will allow relatively rapid two-dimensional (2D) nonlinear analyses of full reinforced concrete buildings. **DOI: 10.1061/(ASCE)ST.1943-541X.0003424.**

Introduction

Over the last century, a great deal of progress has been made by engineers and researchers in their attempts to understand and apply the behavior of cracked concrete to structural design and assessment. Analyses that undergraduates now consider easy to solve were once considered much more challenging. In the 1908 *Cyclopedia of Civil Engineering*, for example, the first sentence about reinforced concrete states, "The theory of flexure in reinforced concrete is exceptionally complicated" (Turneaure 1908, p. 185). It is partly for this reason that they also noted that for typical concrete with an ultimate compressive strength of 14 MPa (2,000 psi), the safety factor should be taken as four and that significant simplifications are required to allow this new material to be used by designers safely.

In the first half of the ensuing century, new analytical methods became available that improved the options for designers, such as the revolutionary analysis method called moment distribution in 1930 (Cross 1930) and the introduction of the limit states concepts in the 1950s, codified by American Concrete Institute (ACI) in 1963 (ACI 1963). The second half of the century saw important additions to the understanding of shear and torsion, including compression field theory (CFT) in 1974 (Mitchell and Collins 1974) and modified compression field theory (MCFT) in 1986 (Vecchio and Collins 1986), which was first implemented in a tangent stiffness form (Adeghe 1986; Stevens 1987), and later in a secant stiffness form into the finite-element method (FEM) by Vecchio (1989, 1990).

The second half of the twentieth century saw even more impressive advances, however, in the potential and capability of digital computers to solve systems of equations. Thus, the number of simultaneous equations that could be solved in a specified time increased by many orders of magnitude during this period.

What is, perhaps, surprising is that these two streams of technological progress of the twentieth century—the improved understanding of the nonlinear behavior of structural concrete and the improvement in computational power—have not fully cross-fertilized in engineering practice. Thus, although engineers use much more powerful computers today than they did in 1990, the structural analyses that these computers are performing today would be familiar to Hardy Cross, the developer of moment distribution in 1930 (Cross 1930).

One potential reason for this separation is that many practicing engineers are hesitant about the use of nonlinear finite-element analysis because there is not yet a consensus on best models or techniques. Most codes, therefore, only allow linear analysis to determine sectional demands in structures. Often, the concern can be traced back to the perception that an engineer can get whatever result they desire from some nonlinear finite-element programs by adjusting input parameters or changing meshes. This was demonstrated in the 2015 prediction contest that preceded the testing of a shear experiment 4,000 mm (13 ft) deep at the University of Toronto because the quality of predictions received before the test was generally poor (Collins et al. 2015). A general pattern in the results was that the more degrees of freedom (DOFs) in the analysis, the worse the overall predictions, although some poor results were obtained with a small number of degrees of freedom as well.

This paper presents an attempt to make a stronger connection between computer power and practical nonlinear analysis of concrete structures for the 21st century. To avoid the problem of "getting whatever results are desired," the method will only include input parameters that are easily measured or defined, such as geometry and material properties, and will use a sharply reduced number of DOFs. This results in a more constrained framework for modeling the behavior of shear-critical reinforced concrete structures, one that is less reliant on the experience level of the user to use correctly as in traditional nonlinear finite-element analysis (Vecchio 2001). The method as presented will allow analysis of

[1]Ph.D. Candidate, Dept. of Civil and Environmental Engineering, Princeton Univ., 54 Olden St., Princeton, NJ 08544 (corresponding author). ORCID: https://orcid.org/0000-0003-0282-6044. Email: ebruun@princeton.edu

[2]Professor, Dept. of Civil and Mineral Engineering, Univ. of Toronto, 35 George St., Toronto, ON, Canada M5S 1A4.

Note. This manuscript was submitted on November 16, 2021; approved on April 15, 2022; published online on July 15, 2022. Discussion period open until December 15, 2022; separate discussions must be submitted for individual papers. This paper is part of the ***Journal of Structural Engineering***, © ASCE, ISSN 0733-9445.

two-dimensional (2D) beams, columns, and frame elements subjected to axial load, moment, and shear. In this paper, the analytical basis and implementation of the model will be shown as applied to the behavior of slender (i.e., relatively long) shear-critical reinforced concrete members. Modeling this type of condition is important because when members fail in shear, they do so in a brittle manner and have little residual capacity.

Basis of Analytical Method

Conventional 2D frame analysis is usually performed using the stiffness method with one-dimensional (1D) elements having three DOFs (Δ_x, Δ_y, and θ) at each end. This works well but has some limitations that the method in this paper will relax. First, the use of a rotational DOF produces an incompatibility in a planar analysis between beams framing into a wall—typically modeled with elements that use two DOFs per node. Although walls may also be represented with frame elements, the challenge then becomes to determine an appropriate nonlinear stiffness when distributed cracking or yielding is expected in the walls at serviceability or ultimate limit states.

A second constraint to using 1D elements is that part of the joint region between beams and columns is modeled as flexible rather than as part of the joint region. This can be rectified by using rigid offsets, but these merely suppress the deformations in the joint region, which may behave differently from simply being rigid. In cases where the joint regions are critical, special element types or methods are required to model them accurately (Birely et al. 2012).

A third limitation is one of convenience: the centerline dimensions used in the geometry of 1D models do not match the overall concrete geometry of the structure because the elements are defined at the elastic neutral axis of the members. A frame that is 10 m wide out-to-out might be modeled as 9.5 m on centers once the geometry of the supporting columns is accounted for; this situation can introduce modeling errors.

To respond to these limitations, the novel element defined in this paper will be based on the gross concrete geometry of the member. Thus a 10-m span out-to-out will be 10 m long in the model as well. Joint regions can be modeled as their own 2D finite elements with their own constitutive relationships as required. However, this paper will focus on the beam/column elements rather than the joint regions.

Fig. 1(a) shows the use of this new element to model a simply-supported reinforced concrete beam. In Fig. 1(b) there are four nodes for each element, with two DOFs per node, or eight DOFs versus six in a conventional 1D frame element. Also, like a 1D element, this new element has a built-in direction to it: the horizontal axis is the longitudinal axis of the member, and the vertical direction is the beam transverse direction. The element is unlike conventional 2D bilinear finite elements, which work the same way if rotated 90°.

The element has been formulated to explicitly represent a gross concrete cross section, where each element can be thought of as a segment of the member being modeled. To satisfy internal equilibrium, distributed internal stresses can only occur on the left and right faces of the element (between Nodes 1 and 2 and between Nodes 3 and 4, respectively). It follows that internal stresses cannot occur on the top or bottom faces of the element (between Nodes 2 and 4 and between Nodes 1 and 3, respectively) because these represent the external faces of the beam.

Fig. 1(c) shows that this element type can accommodate the deformations associated with axial load (N), moment (M), and shear (V). Axial tension will occur with all four horizontal nodal forces pointing outward from the element. Moment is resisted by horizontal nodal forces of opposite signs on the top and bottom of

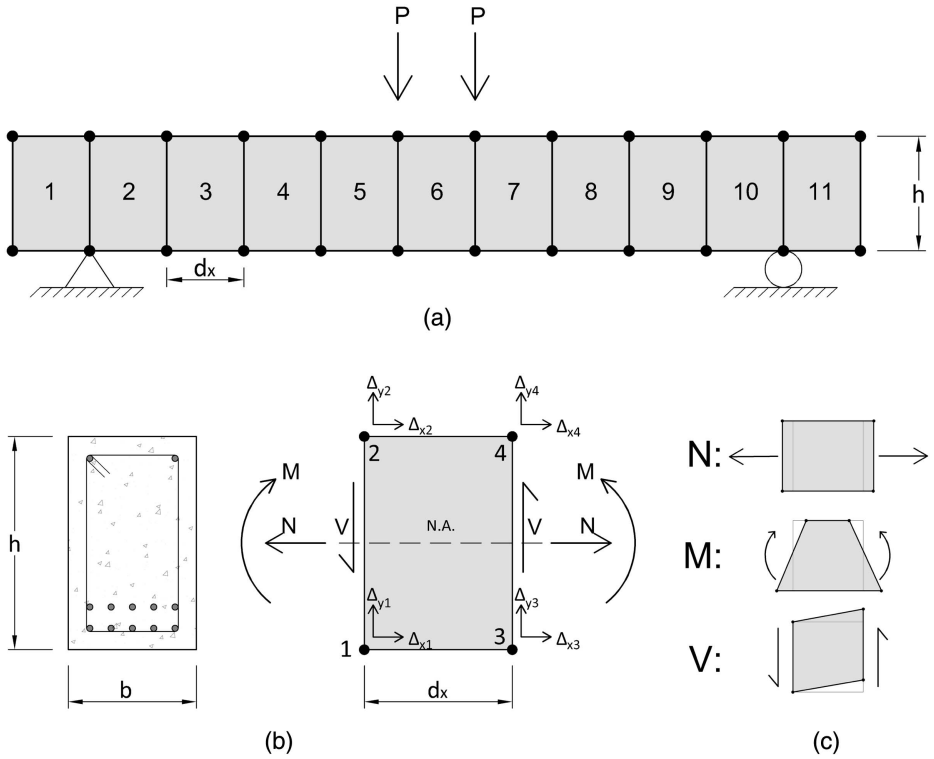

Fig. 1. Use of the novel element presented in this paper: (a) a reinforced concrete beam is represented by a string of elements; (b) each element has eight DOFs; and (c) positive axial, flexure, and shear sign convention.

the member. Shear forces are associated with vertical forces on the sides.

From the definition of the element (summarized in Fig. 1) the following statements can be made:

- Plane sections prior to deformation will remain plane after deformation because the element sides are straight lines.
- Each element must have constant depth because moments will result only from horizontal forces.
- Axial loads will be distributed equally to the top and bottom nodes, making the notional axis of axial load the middle of the gross depth.
- Longitudinal strains are constant along the longitudinal length (d_x) of the element, which means that the elements can be considered constant-moment elements in a sense. Multiple elements along the length of the member [e.g., Fig. 1(a)] will therefore be required to account for moment gradients.
- The shear stresses on the left and right faces will be assumed constant, which means that shear forces are distributed equally to the top and bottom nodes.

A conventional finite element with only four nodes and eight DOFs (i.e., using bilinear interpolation) would result in unacceptable overestimates of stiffness coming from the prediction of spurious shear stresses due to shear locking. At least a cubic order of interpolation functions is recommended to avoid locking, which would result in a 16-node quadrilateral element (Bathe 2014, p. 424). Yet even such an element would not necessarily be able to capture the complex behavior in reinforced concrete members. Therefore, to avoid these issues while remaining computationally simple, the element derived in this paper has been purposely formulated for use in cracked reinforced concrete analysis and does not use conventional finite-element interpolation functions. Instead, the shear stiffness will be decoupled from the flexure and axial-load stiffness, which allows the computational complexity of the element to remain low (four nodes and eight DOFs) while still producing accurate results.

In concept, this is a similar approximation made by shear design methods used in the Canadian Standards Association (CSA) code (CSA 2019) or AASHTO load and resistance factor design (LRFD) (AASHTO 2020) bridge design specifications, where a longitudinal strain, ε_x, calculated from the sectional forces is an input into the shear design equation. To define the overall stiffness matrix for this element, it will be necessary to first define the flexural and shear behavior, and then to combine the separate parts to produce the element.

The paper will first go through the formulation and derivation of the element, followed by a validation study against

- two large slender reinforced concrete experiments for mesh dependency evaluation, and
- the ACI shear-critical slender reinforced concrete beam experimental database (DAfStb) (Reineck et al. 2013, 2014).

Constitutive Relations

In terms of flexure and axial load, the analysis is based on a conventional strain compatibility approach assuming that plane sections remain plane. This portion of the analysis is therefore a conventional fiber model based on uniaxial behavior in the longitudinal direction. Any appropriate material model may be used for this analysis.

The model for shear assumes constant shear stress within the element with a stress that is consistent with the strain state at the centroid of the element. Two-dimensional shear behavior requires three relations to be defined, for example, three strains to form a Mohr's circle of strain, which can then be converted into stresses via a 2D general model of cracked concrete shear behavior. In the element introduced in this paper, the horizontal strain (ε_x) is taken from the flexural strain profile at midheight, which is itself derived from the nodal displacements. The nodal deformations are also used to determine a shear strain (γ_{xy}) as a second condition.

For the third condition required to fully define the 2D shear behavior, rather than using the vertical sides of the element to calculate an average vertical strain, a zero transverse clamping stress condition is instead applied ($f_y = 0$). Thus, the vertical component of the diagonal compression stress must be balanced by vertical components of average principal tensile stress in the cracked concrete plus stirrup forces, if any. This means that the transverse behavior is governed by a stress constraint rather than a displacement constraint. This has the advantage that it removes any sensitivity to the low quality of vertical discretization over the depth of the member. For cases where the clamping stress is known to be nonzero, perhaps near point loads, this can also be accounted for (Acevedo et al. 2009; Uzel 2003), but this topic will not be explored in this paper.

Applying the three conditions for shear defined in the preceding paragraphs (ε_x, f_y, and γ_{xy}) to any suitable 2D general cracked reinforced concrete shear analysis method can provide the relationships between stress and strain for these inputs. In the current paper, Vecchio and Collins's (1986) MCFT is used. Fig. 2 shows the equations that define the theory and will be used to stay compatible with the design codes [i.e., CSA (2019) and AASHTO (2020)] that also use this method for shear design.

Thus, the method described in this paper is consistent with the intentions of a number of codes at least in terms of shear, and can also be made so in terms of flexure and axial load. To apply the shear conditions for a given element shape, the two strains, ε_x and γ_{xy}, are determined from the nodal deformations, and then an iterative loop is run where the transverse strain required to achieve a zero net clamping stress is determined. At this point, the interaction terms are neglected, and the equation $v_{xy} = \bar{G} \cdot \gamma_{xy}$ is used to determine an updated secant value of the shear modulus $\bar{G}$, which will be used in the definition of the portions of the stiffness matrix that result from shear.

Stiffness Matrix Definition

The following subsections will describe the process of deriving the stiffness matrix for the element, which is made up of three components: flexure and axial loads $[K_1]$, shear forces $[K_2]$, and terms to account for the additional demands on longitudinal reinforcement resulting from the web being potentially diagonally cracked $[K_3]$. The final matrix for the element in local coordinates will be defined as the sum of the three submatrices

$$[[K_1] + [K_2] + [K_3]] \begin{Bmatrix} \{\Delta_{x1} \\ \Delta_{y1} \\ \Delta_{x2} \\ \Delta_{y2} \\ \Delta_{x3} \\ \Delta_{y3} \\ \Delta_{x4} \\ \Delta_{y4}\} \end{Bmatrix} = \begin{Bmatrix} F_{x1} \\ F_{y1} \\ F_{x2} \\ F_{y2} \\ F_{x3} \\ F_{y3} \\ F_{x4} \\ F_{y4} \end{Bmatrix} + [FEF] \quad (1)$$

where the nodal deformations and forces are shown in Fig. 1(b). The vector $[FEF]$ represents fixed end forces for self-straining problems as with conventional 1D frame analysis.

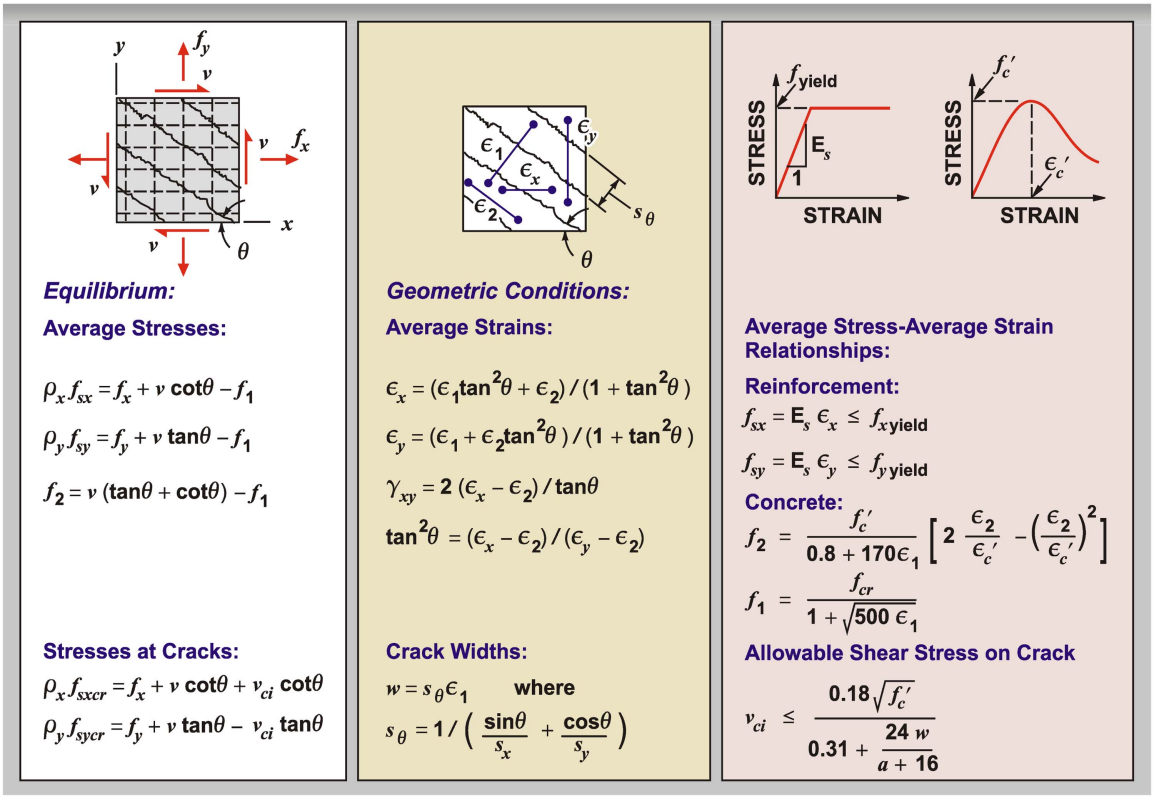

Fig. 2. Equations of the Modified Compression Field Theory (MCFT).

Flexure and Axial Loads

The stiffness method used for the proposed element is based on a secant stiffness approach as recommended by Vecchio and implemented in the VecTor2 2D finite-element analysis program (Vecchio 1990). Starting with a set of nodal displacements, top and bottom average strains are determined as $\varepsilon_{top} = (\Delta_{x4} - \Delta_{x2})/d_x$ and $\varepsilon_{bot} = (\Delta_{x3} - \Delta_{x1})/d_x$, and at other elevations the strains vary linearly. Fig. 3 shows these strains.

These strains are then applied at multiple layers in the section to determine the uniaxial stress at each layer of concrete or steel using a conventional strain compatibility or fiber model approach, as shown in Fig. 4.

From the concrete and steel reinforcement stresses over the depth [Fig. 4(a)], a secant stiffness is determined at each layer [Fig. 4(b)]. Thus, the longitudinal secant stiffness for concrete is taken as $\bar{E}_{c,i} = f_{c,i}/\varepsilon_{c,i}$ at each given layer i, where $f_{c,i}$ is the calculated concrete stress and $\varepsilon_{c,i}$ is the longitudinal strain in this layer. For cases where $\varepsilon_{c,i}$ is close to zero, the initial uncracked tangent stiffness of the concrete, E_c, should be used for $\bar{E}_c$. When using tension stiffening relationships for average concrete tensile stresses on the tension side, there must also be a crack check to ensure average tensile stresses can be carried across any flexural crack if flexural yield is possible. Because this paper is about shear failures, this will not be discussed in detail here, but has been discussed by Bentz (2000b).

Converting the longitudinal secant stress stiffness distribution, $\bar{E}$, to entries in a stiffness matrix requires deriving a relationship between force and displacement at each node. Recall the definition of stiffness as it applies to the stiffness method: force per unit displacement. Thus K_{ij} is the term in the stiffness matrix that corresponds to the force at DOF i resulting from a unit displacement at DOF j while keeping all other displacements at zero. Column j of the stiffness matrix can be thought of as the reaction forces required in all DOFs to keep the free-body diagram in equilibrium as a response to a unit deformation in the jth DOF.

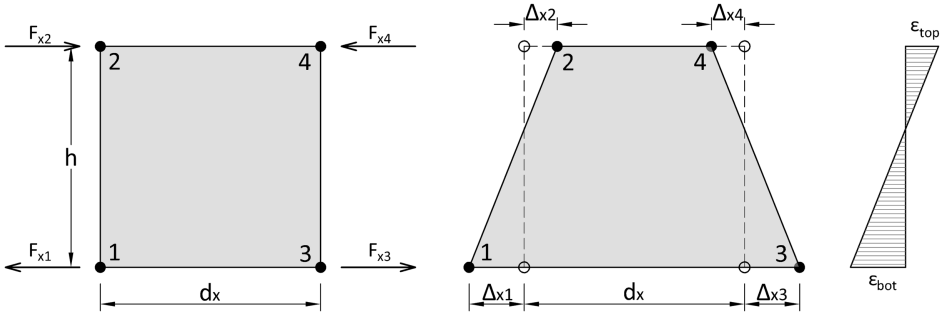

Fig 3. Flexure is represented by the relative deformation of the top and bottom nodes in the element.

J. Struct. Eng., 2022, 148(9): 04022142

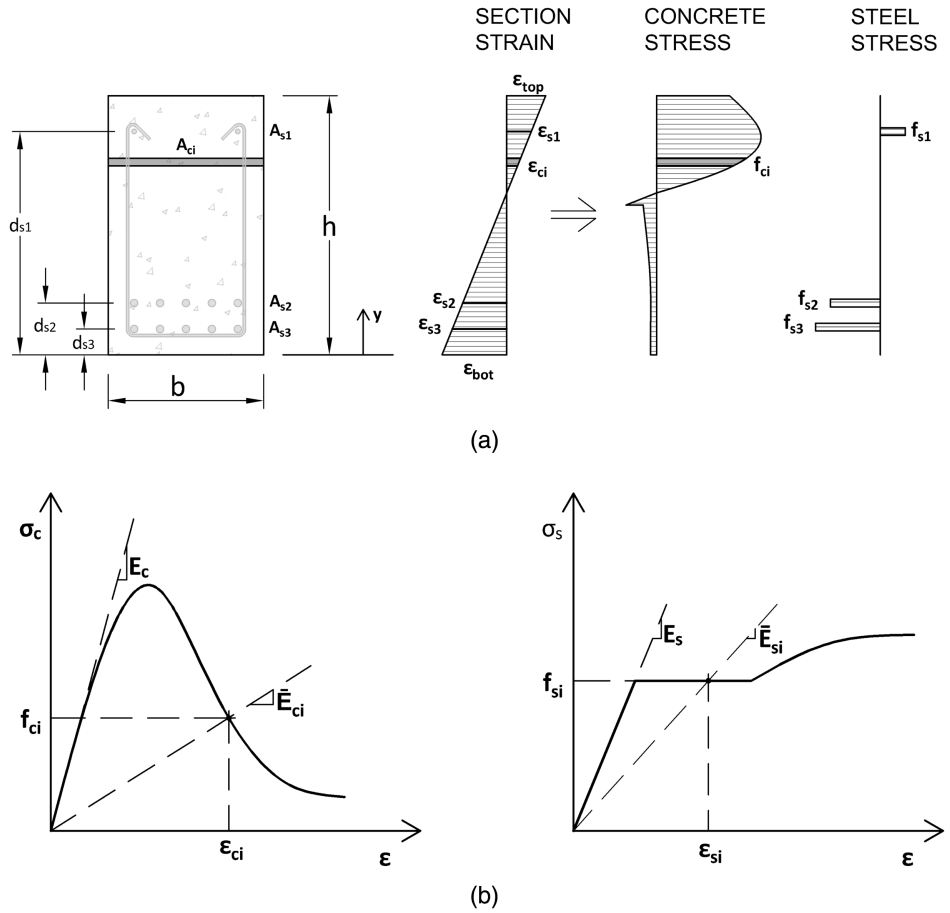

Fig. 4. (a) Reinforced concrete cross-section as a series of layers, also known as a fiber model, where each layer of the cross-section is represented using a secant stiffness for concrete and steel; and (b) each layer of the cross section is represented using a secant stiffness for concrete and steel.

An incremental unit displacement is applied at DOF 1 (i.e., $u_1 = 1$) while keeping the deformations of all other nodes constant, results in a linear increment to the current sectional strain profile ($d\varepsilon_{\text{bot}}$ in Fig. 5). This is a fictitious additional displacement that is only applied at DOF 1 (and zero elsewhere), with the pre-existing strain profile coming from previously calculated nodal displacements. For example, in Fig. 5, this pre-existing condition is shown as compression at the bottom and tension at the top. This method allows the evaluation of the flexural/axial stiffness terms in its current deformed state. F_B and F_T in Fig. 5 are changes to the existing nodal forces as a result of this fictitious additional displacement. These forces are then used to determine the stiffness terms, K_B and K_{TB}, in Eq. (2), which will be used in the stiffness matrix $[K_1]$. K_{TB} can be thought of as a cross-stiffness term, meaning that an action that occurs at the bottom of the section will have an influence on the top (and vice versa for K_{BT}), which is an intuitive result for a solid body

$$K_B = \frac{\Delta F_{x1}}{u_1} = \frac{F_B}{d\varepsilon_{\text{bot}} \cdot d_x}$$
$$K_{TB} = \frac{\Delta F_{x2}}{u_1} = \frac{F_T}{d\varepsilon_{\text{bot}} \cdot d_x} \tag{2}$$

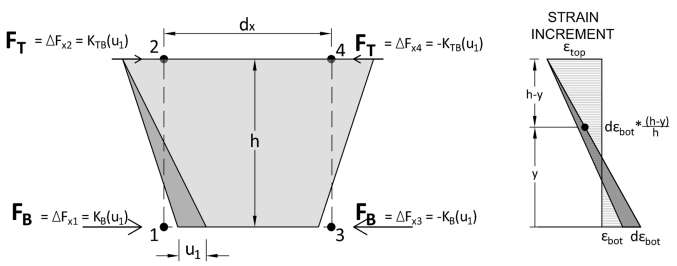

Fig. 5. Incremental change in horizontal forces at all nodes as a result of a unit displacement in DOF 1 (i.e., $u_1 = 1$).

The total axial force in the cross section as a result of this displacement increment is calculated as the product of the secant stiffness and the resulting strain increment, which varies linearly with depth, integrated over the full cross-section area [Eq. (3)]

$$F = \int_A \bar{E}\varepsilon \cdot dA = \int_0^h \bar{E} \cdot d\varepsilon_{\text{bot}} \frac{h-y}{h} \cdot b \cdot dy$$
$$= \frac{d\varepsilon_{\text{bot}}}{h} \int_0^h \bar{E} \cdot (h-y) \cdot b \cdot dy \tag{3}$$

For practical purposes, this calculation can also be discretized by representing the cross section as a collection of constant-strain layers. But if the discretization is too coarse, instabilities related to cracking of concrete can arise (Bentz 2000b).

The equivalent nodal force is then found through moment equilibrium in the section, as shown in Eq. (4). For example, the force in the bottom node should have the same moment about the top node as the sum of the force components in the section (and vice versa for the force in the top node)

$$F_B \cdot h = M_T = \frac{d\varepsilon_{\text{bot}}}{h} \int_0^h \bar{E} \cdot (h-y)^2 \cdot b \cdot dy$$
$$F_T \cdot h = M_B = \frac{d\varepsilon_{\text{bot}}}{h} \int_0^h \bar{E} \cdot (h-y) y \cdot b \cdot dy \quad (4)$$

Substituting Eq. (4) into Eq. (2) results in the following equations for the stiffnesses:

$$K_B = \frac{1}{d_x \cdot h^2} \int_0^h \bar{E} \cdot (h-y)^2 \cdot b \cdot dy$$
$$K_{TB} = \frac{1}{d_x \cdot h^2} \int_0^h \bar{E} \cdot (h-y) y \cdot b \cdot dy \quad (5)$$

Performing the same set of calculations—with a displacement at Node 2 instead—would produce the same values for K_{BT} as K_{TB}. The value of K_T, which represents the relationship between the force F_T and Δ_{x2}, is the following:

$$K_T = \frac{1}{d_x \cdot h^2} \int_0^h \bar{E} \cdot y^2 \cdot b \cdot dy \quad (6)$$

To summarize, these calculations show that bottom areas of the cross section contribute more to the stiffness of the bottom DOFs and vice versa [i.e., $(h-y)^2$ and y^2 scaling for K_B and K_T, respectively]. On the other hand, the K_{BT} and K_{TB} cross-stiffness terms represent the inherent connectivity in a concrete cross section: any single region, for example the bottom, will contribute to the stiffness throughout the whole cross section.

The contribution of steel reinforcement to the flexural and axial stiffness terms (K_B, K_T, K_{BT}, and K_{TB}) is calculated using the discrete forms of Eqs. (5) and (6): summing the areas of the bars multiplied by the secant steel stiffness, $\bar{E}_s$, and depth, d_s, in the cross section.

In addition to the horizontal-direction stiffness terms, a stiffness is also required to restrain the relative value of vertical displacements of the top and bottom nodes. Because a stress condition is used in the shear model rather than strains based on nodal deformations, the vertical stiffness terms need not be detailed. To provide an appropriate stiffness for the behavior of a beam embedded within a wall carrying vertical compression, the following relationship is recommended for K_v, where E_c is taken as the initial tangent stiffness of the concrete multiplied by the tributary area of the element (i.e., half the width):

$$K_v = E_c \frac{b \cdot d_x}{2h} \quad (7)$$

Combining these terms produces the $[K_1]$ matrix [Eq. (8)], which represents the axial/flexural stiffness of the element. From the derivation, it follows that this matrix is symmetric and that a force on one face of the element is mirrored on the other face to maintain equilibrium

$$[K_1] = \begin{bmatrix} K_B & 0 & K_{BT} & 0 & -K_B & 0 & -K_{BT} & 0 \\ 0 & K_V & 0 & -K_V & 0 & 0 & 0 & 0 \\ K_{TB} & 0 & K_T & 0 & -K_{TB} & 0 & -K_T & 0 \\ 0 & -K_V & 0 & K_V & 0 & 0 & 0 & 0 \\ -K_B & 0 & -K_{BT} & 0 & K_B & 0 & K_{BT} & 0 \\ 0 & 0 & 0 & 0 & 0 & K_V & 0 & -K_V \\ -K_{TB} & 0 & -K_T & 0 & K_{TB} & 0 & K_T & 0 \\ 0 & 0 & 0 & 0 & 0 & -K_V & 0 & K_V \end{bmatrix} \quad (8)$$

The initial value of this matrix for a new analysis can be derived from the initial uncracked state, where $\bar{E}_c$ is taken as E_c for all depths. Using this matrix, the new strain state for a target load or deformation can be determined. This will then require re-evaluation of the stiffness terms in an iterative solution. Convergence is obtained when each of the the K_T, K_B, and K_{TB} values for each element are sufficiently close from one iteration to the next. For efficient solutions, it is useful to solve the entire multielement finite-element model at a time and check the convergence ratios afterward, taking the worst convergence of any element as the measure of overall convergence. By itself, however, matrix $[K_1]$ is singular because there is not yet any shear stiffness in the model.

Shear Forces

A similar process to that used in the preceding section will be followed for shear: (1) the strain state is determined from the nodal deformations, (2) the secant shear stiffness is evaluated using an MCFT formulation, and (3) a shear stiffness matrix is populated. This matrix, $[K_2]$, is then added to the flexure and axial stiffness matrix $[K_1]$.

The shear stress in the element is assumed to be constant, meaning that under shear alone, the rectangular element will deform into a parallelogram as shown in Fig. 1(c). The shear stress will be assumed to only be carried by the member web width, b_w, and the effect of any flanges (as in a T-section) on shear will be neglected, as is typical for design codes.

Shear strains are a component of the total deformation of the element. It is therefore necessary to isolate the shear strains from an arbitrary displaced shape. Consider building up the components of vertical deformation at Node 3 as shown in Fig. 6.

Taking Node 1 as the origin, consider that a rigid-body rotation [Fig. 6(b)] will be associated with a horizontal deformation at Node 2 of $\Delta_{x2} - \Delta_{x1}$, and a vertical displacement at Nodes 3

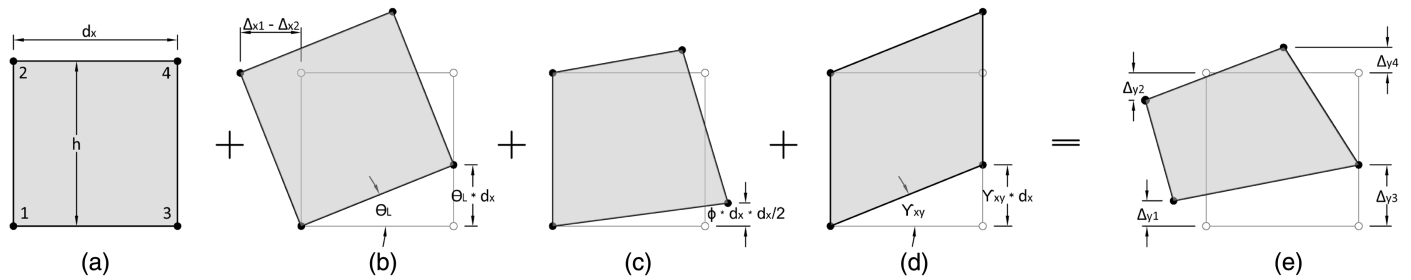

Fig. 6. (a) Undeformed; (b) rotation; (c) flexure; and (d) shear deformations used to represent (e) relative vertical displacements of the element.

and 4 of $\theta_L \cdot d_x$, where θ_L is member rotation at the left side of the element [Eq. (9)]

$$\theta_L = \frac{\Delta_{x2} - \Delta_{x1}}{h} \tag{9}$$

In addition to rigid-body rotation, and independently, the member may also show curvatures due to moments. These are defined as the gradient in longitudinal strain with depth [Eq. (10)]

$$\phi = \frac{\varepsilon_{\text{bot}} - \varepsilon_{\text{top}}}{h} = \frac{(\Delta_{x3} - \Delta_{x1}) - (\Delta_{x4} - \Delta_{x2})}{h \cdot d_x} \tag{10}$$

The influence of a constant curvature on the vertical displacement at Node 3 can be found from the second-moment area theorem as $(\phi \cdot d_x \cdot d_x/2)$.

Uniform horizontal displacements at Nodes 3 and 4 (axial loads) will not be associated with vertical deformations at Node 3, but shear strains will be. Thus, any shear strain within the element will produce a vertical deformation at Node 3 due to shear of $\gamma_{xy} \cdot d_x$ as shown in Fig. 6(d).

Combining these components together and accounting for the deformation of Node 1 [Fig. 6(e)] means the modeled change in y displacement, $\Delta_{y3} - \Delta_{y1}$, must equal the sum of the aforementioned components. Using the average vertical displacements of both nodes at each side results in Eq. (11)

$$\underbrace{\frac{\Delta_{y3} + \Delta_{y4}}{2}}_{\text{Avg.Right}} - \underbrace{\frac{\Delta_{y1} + \Delta_{y2}}{2}}_{\text{Avg.Left}} = \underbrace{\theta_L \cdot d_x}_{\text{Rotation}} + \underbrace{\phi d_x \cdot \frac{d_x}{2}}_{\text{Curvature}} + \underbrace{\gamma_{xy} \cdot d_x}_{\text{Shear}} \tag{11}$$

Solving for γ_{xy} in Eq. (11) results in Eq. (12) for shear strain given arbitrary nodal displacements. Eq. (12) is also produced as the sum of shear strains at the centroid of the element produced by changing each DOF in turn

$$\gamma_{xy} = -\frac{\Delta_{x1}}{2h} - \frac{\Delta_{y1}}{2d_x} + \frac{\Delta_{x2}}{2h} - \frac{\Delta_{y2}}{2d_x} - \frac{\Delta_{x3}}{2h} + \frac{\Delta_{y3}}{2d_x} + \frac{\Delta_{x4}}{2h} + \frac{\Delta_{y4}}{2d_x} \tag{12}$$

This shear strain, along with the longitudinal strain at middepth, ε_x, from the flexural calculations is used in the following constitutive relationship for shear:

$$\begin{bmatrix} k_{11} & k_{12} & k_{13} \\ k_{21} & k_{22} + k_s & k_{23} \\ k_{31} & k_{32} & k_{33} \end{bmatrix} \begin{Bmatrix} \varepsilon_x \\ \varepsilon_y \\ \gamma_{xy} \end{Bmatrix} = \begin{Bmatrix} f_{cx} \\ 0 \\ v_{xy} \end{Bmatrix} \tag{13}$$

where k_s = stiffness of the stirrup steel (product of secant stiffness of steel and stirrup percentage). This matrix is the secant shear stiffness matrix of cracked concrete, with the definition and solution technique described by Vecchio (1990). In solving for the unknown transverse strain, ε_y, the zero clamping stress condition is applied, as shown in the right side of Eq. (14). Thus, the following expression must be solved for the value of the unknown transverse strain, ε_y:

$$k_{21} \cdot \varepsilon_x + (k_{22} + k_s) \cdot \varepsilon_y + k_{23} \cdot \gamma_{xy} = 0 \tag{14}$$

Although only one strain is changing in this calculation, the stiffness matrix terms depend on this strain via changes in the angle of principal compression θ, stirrup stress, and the corresponding secant stiffnesses, $\bar{E}_{c2}$ and $\bar{E}_{c1}$ [principal compression and tension, respectively (Vecchio 1990)]. Thus, the solution of this equation must be iterative because new values of ε_y will update the secant stiffnesses, and therefore, the k_{21}, k_{22}, and k_{23} values seen in Eq. (14). The value of ε_y will be converged when the two secant stiffnesses ($\bar{E}_{c1}$ and $\bar{E}_{c2}$) have stabilized from one iteration to the next.

This converged strain state should be solved for each time the stiffness matrix of an element is required because the converged results in Eq. (13) are needed to generate the $[K_2]$ and $[K_3]$ matrices. The calculated ε_y is the appropriate value to use when considering the transverse strain in the member, and the vertical deformation of the nodes should not be used in evaluating the vertical strains. Instead of using the MCFT formulation for the element as outlined in this section, the shear stiffness of cracked reinforced concrete can be determined based on other existing constitutive models (Vecchio et al. 2001; Maekawa et al. 2003; Kaufmann and Marti 1998).

With the strain state solved for, the converged shear stress and strain values can be related through the secant shear stiffness ($\bar{G}$)

$$v_{xy} = \bar{G} \cdot \gamma_{xy} \tag{15}$$

This value of $\bar{G}$ will be used in the generation of the stiffness matrix $[K_2]$. The right side of Eq. (13) shows in the top row, a value of f_{cx} that is also generated by this shear analysis. This represents the longitudinal components of concrete compression and tension stiffening that are required to hold the element to the given strain state with zero clamping. This interaction term between shear and longitudinal forces is important after diagonal cracking and will be further discussed in the section "Impact of Diagonal Cracking" as the basis for matrix $[K_3]$.

Substituting the shear strain [Eq. (12)] into Eq. (15) results in an expression for shear stress in terms of nodal displacements and the secant shear stiffness. Fig. 7 shows the conversion from applied shear stress to nodal forces based on the assumption of constant shear stress in the element.

To be consistent with observed behavior and codes, a final correction must be made before generating the stiffness matrix $[K_2]$. The definition of shear stresses in Fig. 7 shows that the stress is applied over the full depth of the member, h, and this is not consistent with the behavior of cracked reinforced concrete (Collins and Mitchell 1997). To a first approximation, shear is carried in reinforced concrete member over a shear depth, d_v, which is defined as the distance between the centroid of flexural compressive forces and the centroid of flexural tensile forces.

The value of d_v used with this element will be taken from codes (CSA 2019; AASHTO 2020) as $d_v = 0.9d$ where d is the effective depth of the member to the tensile reinforcement but need not be taken as less than $0.72h$. To account for this, the shear stiffness from the constitutive model must be converted from the shear depth, d_v, to the full member depth, h, while keeping the moment

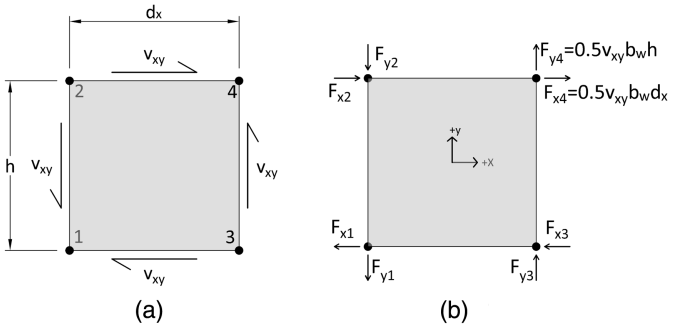

Fig. 7. (a) Positive shear stress on an element; and (b) resulting nodal forces in terms of shear stress.

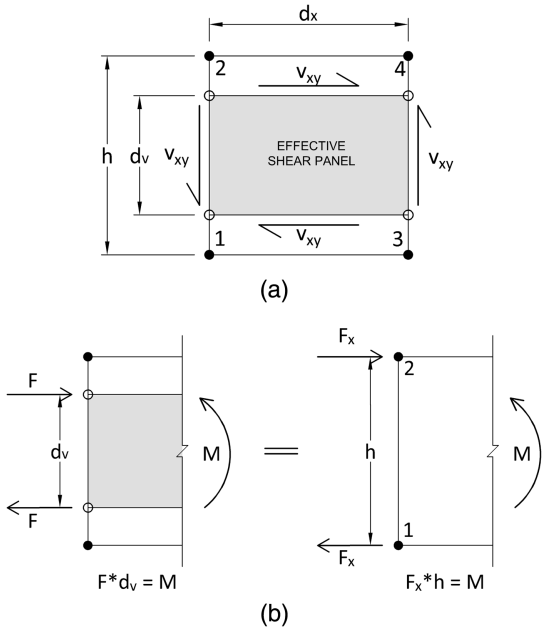

Fig. 8. (a) Shear stress acting on the effective panel area; and (b) transforming the horizontal shear force while maintaining moment equivalency.

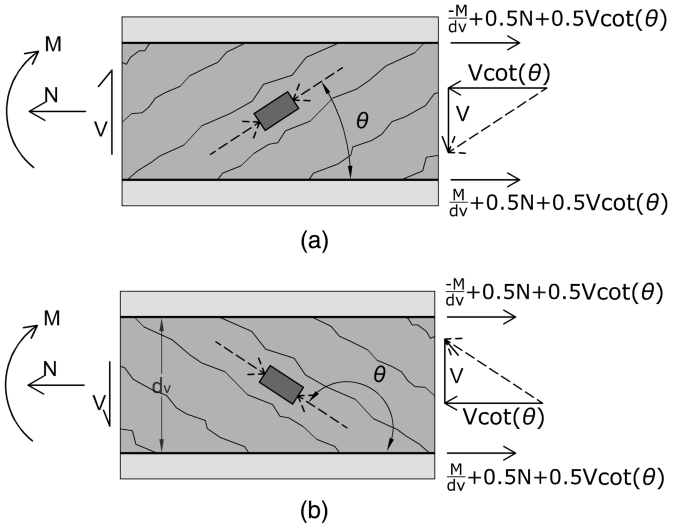

Fig. 9. Contributions to tension in top and bottom chords in a code-based shear model for (a) negative shear; and (b) positive shear.

on the section the same ($F \cdot d_v = F_x \cdot h$ as shown in Fig. 8). In practice, this means that when using the shear stiffness to generate the stiffness matrix $[K_2]$, the value of $\bar{G}$ must be multiplied by the ratio of d_v/h.

Putting all these pieces together leads to the $[K_2]$ matrix, which relates shear deformations to nodal forces and therefore represents the shear stiffness of the element

$$[K_2] = \frac{\bar{G} b_w d_v}{4h} \cdot \begin{bmatrix} \frac{d_x}{h} & 1 & -\frac{d_x}{h} & 1 & \frac{d_x}{h} & -1 & -\frac{d_x}{h} & -1 \\ 1 & \frac{h}{d_x} & -1 & \frac{h}{d_x} & 1 & -\frac{h}{d_x} & -1 & -\frac{h}{d_x} \\ -\frac{d_x}{h} & -1 & \frac{d_x}{h} & -1 & -\frac{d_x}{h} & 1 & \frac{d_x}{h} & 1 \\ 1 & \frac{h}{d_x} & -1 & \frac{h}{d_x} & 1 & -\frac{h}{d_x} & -1 & -\frac{h}{d_x} \\ \frac{d_x}{h} & 1 & -\frac{d_x}{h} & 1 & \frac{d_x}{h} & -1 & -\frac{d_x}{h} & -1 \\ -1 & -\frac{h}{d_x} & 1 & -\frac{h}{d_x} & -1 & \frac{h}{d_x} & 1 & \frac{h}{d_x} \\ -\frac{d_x}{h} & -1 & \frac{d_x}{h} & -1 & -\frac{d_x}{h} & 1 & \frac{d_x}{h} & 1 \\ -1 & -\frac{h}{d_x} & 1 & -\frac{h}{d_x} & -1 & \frac{h}{d_x} & 1 & \frac{h}{d_x} \end{bmatrix} \quad (16)$$

Impact of Diagonal Cracking

The results obtained using the matrix $[K_1]$ for flexure and axial loads plus $[K_2]$ for shear forces will produce good estimates of strength and stiffness prior to diagonal shear cracking but will provide unconservative estimates of demand on the longitudinal reinforcement after diagonal cracking. To understand why, consider Fig. 9, which shows free-body diagrams with sectional forces on the left and simplified force demands on the top and bottom chords and web of the member on the right sides. After diagonal cracking, shear is carried primarily by diagonal compression in the web between the cracks (Vecchio and Collins 1986), and while the vertical component of this diagonal compression carries the shear, the horizontal component must also be resisted. Prior to diagonal cracking, the force component from the principal tensile stress direction will cancel out these horizontal reactions, but these will no longer balance after diagonal cracking. The additional force demand from shear is calculated as $V \cdot \cot(\theta)$, as shown in Fig. 9, if the average residual tensile stresses from tension stiffening in the web are neglected, which is the case with design codes.

In the constitutive model for shear [Eq. (13)] this additional longitudinal demand is represented by the term f_{cx}. This term can be thought of as the additional longitudinal compressive stress required to hold the strain state to the assumed values under the given shear loading. The first equilibrium equation of the MCFT in Fig. 2 shows that when using average stresses, this longitudinal component is calculated as:

$$\rho_x \cdot f_{sx} = f_x + v \cdot \cot\theta - f_1 \quad (17)$$

where the left side of the equation gives the average demand on the longitudinal reinforcement and the right side of the equation is the term f_{cx} in Eq. (13). The challenge with using this equation is the allocation of the term f_x, which represents the average X-direction stress that the shear region carries from the combined effects of axial load, prestressing, and moment. Assuming this value to be zero because the shear panel is near the neutral axis and is only intended to carry shear forces, the equation can be rearranged as follows:

$$\rho_x \cdot f_{sx} + f_1 = v \cdot \cot\theta \quad (18)$$

The left side of the equation contains the average steel and concrete stresses that have already been accounted for in the axial and flexural analysis that produced $[K_1]$. The right side of the equation shows the additional demand on the longitudinal reinforcement, similar to that shown in Fig. 9.

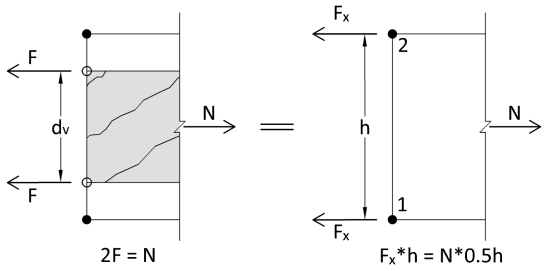

Fig. 10. Transforming the horizontal chord force acting on the reduced area to the nodal position.

This additional demand on the longitudinal reinforcement could be accounted for as an equivalent axial force applied to the flexural- and axial-load analysis. But this would produce convergence issues because the source of this force would be the shear analysis, and the resistance would be the flexural analysis and the two are tied together. To avoid this disconnect, this longitudinal effect of shear stress is better included directly in the shear stiffness matrix. Because this will result in the same sectional forces causing larger strains than previously obtained, this additional matrix $[K_3]$ will produce stiffness which subtracts from $[K_2]$ in the longitudinal direction. With the additional stress demand as $v \cdot \cot(\theta)$, the shear area as $d_v \cdot b_w$, and an equal distribution of force between the top and bottom node, the X-direction tension force at each node on the right face can be expressed as:

$$F_x = 0.5 \cdot d_v \cdot b_w \cdot \cot\theta \cdot \bar{G} \cdot \gamma_{xy} \tag{19}$$

The $[K_3]$ matrix expresses the effects of the additional longitudinal demands from shear stresses [Eq. (20)] and is obtained by substituting the equation for shear strain [Eq. (12)] into Eq. (19). Tension is always added to the chords (i.e., left face = negative sign and right face = positive sign) irrespective of the shear deformation because the product of $\cot(\theta)$, and γ_{xy} is always negative

$$[K_3] = A \cdot \begin{bmatrix} -\frac{1}{h} & -\frac{1}{d_x} & \frac{1}{h} & -\frac{1}{d_x} & -\frac{1}{h} & \frac{1}{d_x} & \frac{1}{h} & \frac{1}{d_x} \\ 0 & 0 & 0 & 0 & 0 & 0 & 0 & 0 \\ -\frac{1}{h} & -\frac{1}{d_x} & \frac{1}{h} & -\frac{1}{d_x} & -\frac{1}{h} & \frac{1}{d_x} & \frac{1}{h} & \frac{1}{d_x} \\ 0 & 0 & 0 & 0 & 0 & 0 & 0 & 0 \\ \frac{1}{h} & \frac{1}{d_x} & -\frac{1}{h} & \frac{1}{d_x} & \frac{1}{h} & -\frac{1}{d_x} & -\frac{1}{h} & -\frac{1}{d_x} \\ 0 & 0 & 0 & 0 & 0 & 0 & 0 & 0 \\ \frac{1}{h} & \frac{1}{d_x} & -\frac{1}{h} & \frac{1}{d_x} & \frac{1}{h} & -\frac{1}{d_x} & -\frac{1}{h} & -\frac{1}{d_x} \\ 0 & 0 & 0 & 0 & 0 & 0 & 0 & 0 \end{bmatrix} \tag{20}$$

where

$$A = \frac{d_v \cdot b_w \cdot \cot\theta \cdot \bar{G}}{4}$$

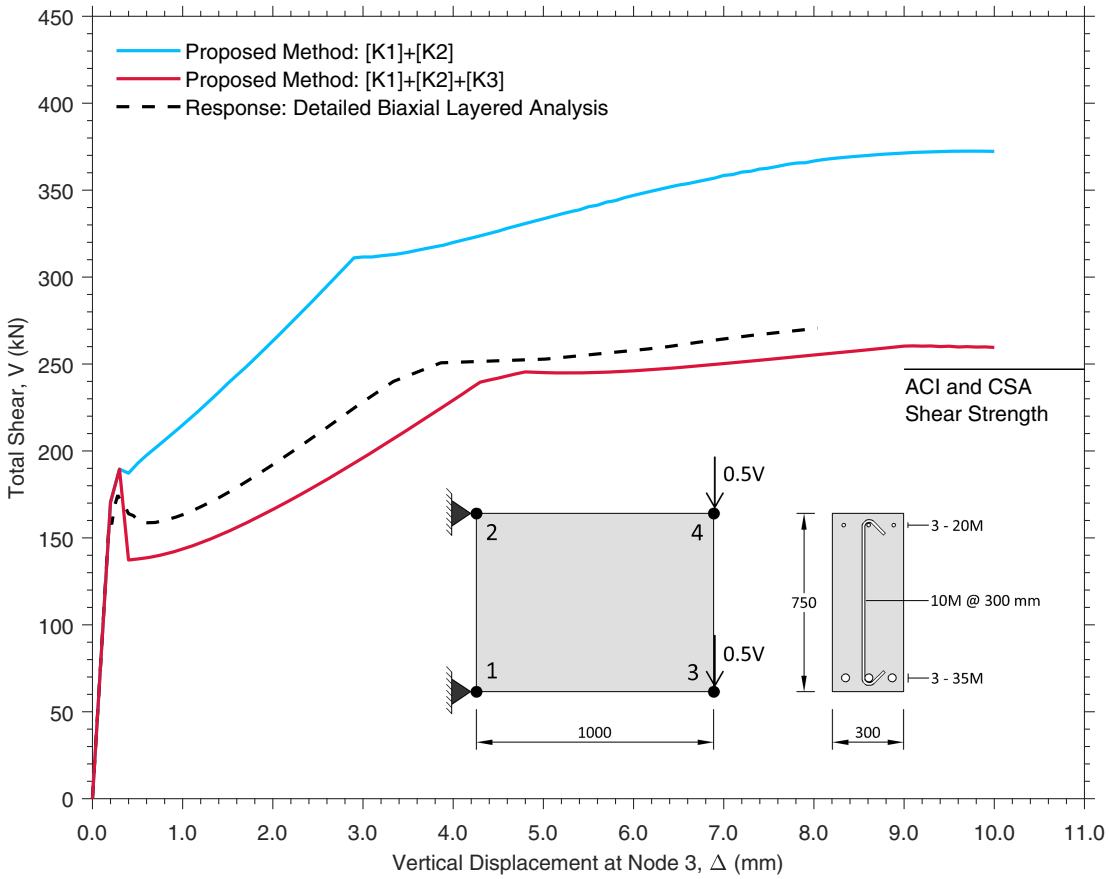

Fig. 11. Single-element analysis of 1-m-long cantilever with shear force V.

J. Struct. Eng., 2022, 148(9): 04022142

While the forces are again being transformed from the reduced shear area to the element nodes (Section 4 discusses this), a correction factor of d_v/h should not be applied. This is because solving the equilibrium condition shown in Fig. 10 results in $F_x = F$, which is different from the equilibrium condition illustrated in Fig. 8.

As is clear, matrix $[K_3]$ is not symmetric because the longitudinal effects of shear are only applied in the X-direction. The components in the vertical direction are neglected because the zero clamping condition already accounted for deformation in that direction. If these terms were retained in the matrix, it would still not be symmetric. Thus, although the inclusion of this longitudinal demand from shear into its own matrix does allow better convergence, it does so at the cost of making the matrix nonsymmetric.

With $[K_3]$ defined, it is now possible to generate the full stiffness matrix as shown in Eq. (1).

Validation of Shear Assumptions

To determine the appropriateness of the assumption that f_x in Eq. (17) can be accurately taken as zero, consider the analyses summarized in Fig. 11. These analyses are of a single-element cantilever fixed on the left and with a distributed vertical force V applied to the right-side nodes. The reinforced concrete member being analyzed contains 900 mm^2 of 500-MPa yield strength tension reinforcement on the top and about 1.5 times code specified minimum stirrups [ACI Committee 318 (ACI 2019); CSA 2019]. The concrete has an ultimate cylinder strength of 32 MPa with a 19-mm specified coarse-aggregate size. The yielding flexural capacity of this member based on a strain compatibility analysis (Bentz 2000a, b) is 326 kN · m. Because the element derivation produces a constant internal bending moment, this moment capacity can be considered valid at the middle of the element giving a maximum shear associated with flexural yield of $326 \cdot 2 = 652$ kN, or off the top of the graph in Fig. 11. The ACI code calculates that the shear strength should be 256 kN, whereasthe CSA code predicts a shear strength of this element of 251 kN. Thus, this member should be expected by the proposed finite-element model to fail in shear at a load V of ~250 kN.

If the behavior of this one-element cantilever is analyzed using only stiffness matrices $[K_1]$ and $[K_2]$, that is, neglecting the influence of diagonal cracking, the top line in the graph is obtained. The subtle change of slope at $V = 160$ kN is associated with flexural cracking whereas the change in slope at $V = 190$ kN is associated with shear cracking. The further change of slope when the shear reaches 311 kN is associated with yield of the stirrups and the peak strength is associated with crushing of the concrete in diagonal compression due to shear, which is how the MCFT predicts shear failures of members with stirrups. Thus, this model with only $[K_1]$ and $[K_2]$ does predict a shear failure but at a force too high when compared with design codes.

If, instead, the analysis is performed as intended with $[K_1]$, $[K_2]$, and $[K_3]$, the lower solid line in Fig. 11 is obtained. This analysis shows the same flexural and shear cracking behavior, but afterward, the additional longitudinal forces included via matrix $[K_3]$ cause much lower stiffness after cracking and a lower shear strength. Indeed the predicted shear strength of 261 kN is very close to both the ACI and CSA shear strengths, showing the importance of matrix $[K_3]$ and suggesting that the assumptions in making this matrix are appropriate.

As a final check of the assumptions, the dashed line in Fig. 11 shows the predictions from the computer program RESPONSE (Bentz 2000b). This sectional analysis program uses about 100 dynamically assigned biaxial concrete layers in the analysis and solves for the analytical shear stress distribution that results from the constitutive model and equilibrium (Jouravski 1856). Unlike the proposed element, RESPONSE makes no assumptions about the value of the term f_x [Eq. (17)] in its analyses. The result is shown in Fig. 11 to be similar to the method proposed in this paper with similar strength and ductility, but somewhat higher stiffness between diagonal cracking and stirrup yield. That the RESPONSE line is reasonably close to the proposed method line suggests that the assumptions behind the new method are appropriate. Details of the constitutive model used in this example are given in the Appendix.

Strategies for Analysis

The flowchart in Fig. 12 details the computational procedure that is followed in a program that implements the element.

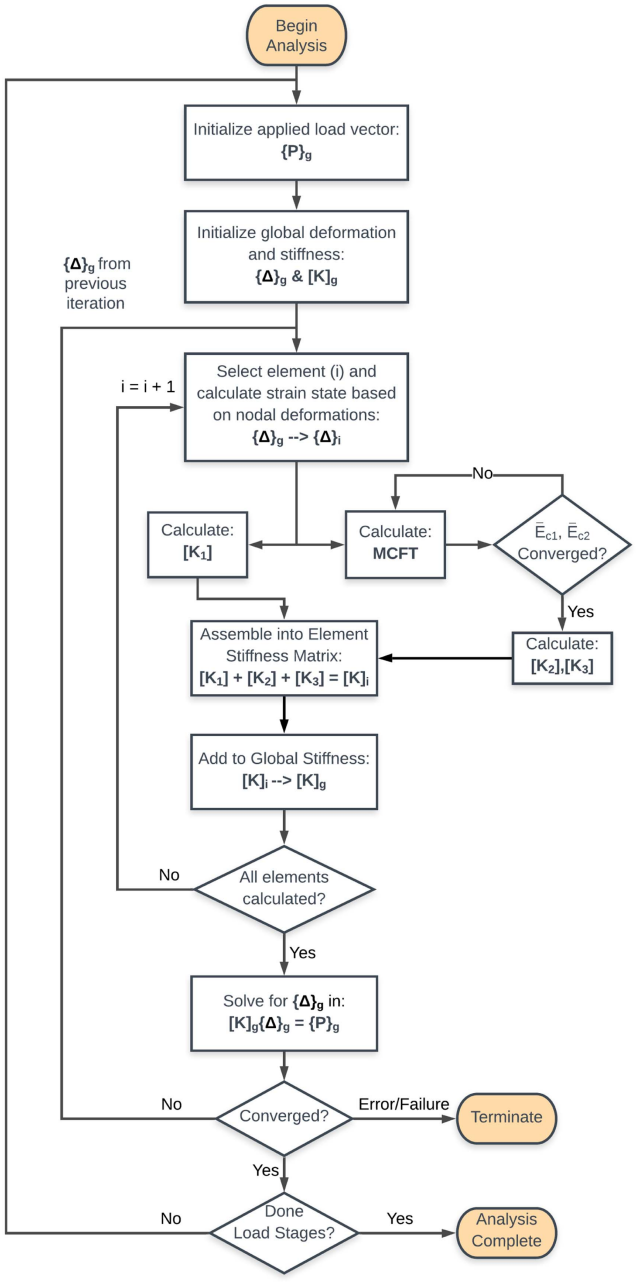

Fig. 12. Analysis process flowchart.

Validation of Element

Although Fig. 11 compared the analysis results with codes, it is also necessary to compare the proposed analysis method with experimental results. This will be performed via a mesh sensitivity study against a pair of tests (Sherwood et al. 2007; Sherwood 2008), followed by a comparison with a database of test results (Reineck et al. 2013, 2014).

Mesh Sensitivity Study

To examine mesh sensitivity and ability to model the shear behavior of slender reinforced concrete members, consider the two shear experiments in Figs. 13 and 14. These experiments were performed at the University of Toronto by Sherwood et al. (2007) and Sherwood (2008). Included here are Specimens L-10H and L-10HS, where the former did not contain shear reinforcement and the second test contained minimum shear reinforcement. Both tests were a total of 9 m long and 1.51 m deep with a concrete strength of 72 MPa and contained flexural reinforcement as shown in Fig. 14. Both beams were tested monotonically under three-point bending and were meant to represent 300-mm-wide strips cut from one-way slabs. Both members failed in shear, with Fig. 13 showing L-10HS after shear failure, with Sherwood present for a sense of scale.

In the analysis of these beams, shown in Fig. 14, a total of 54 elements were used between the supports along with an additional three elements on each end beyond the supports. Self-weight was applied as constant nodal loads, and the displacement of the top node was incrementally lowered until the peak strength was ascertained. The beam geometries and reinforcement (Sherwood 2008) are shown in cross section in Fig. 14, and this geometry was used for the majority of the length of the member. Near the point load, however, a modified member type (explicitly defined and assigned by the user) was used to force any shear failure to occur at the critical section for shear, at a distance of the effective depth, d, from the point load. Thus, within a distance of 1,400 mm of the point load, the stirrup yield stress was doubled for Beam L-10HS, whereas minimum stirrups were added to the same region of Beam L-10H. This way the member would crack in shear and flexure near the point load but a shear failure would be suppressed at these locations. The reason codes indicate that the critical section for shear is away from the point load is that failure is predicted to occur by sliding on a diagonal crack, and this is not physically possible to occur exclusively within a narrow vertical element near the point load. This method of suppressing shear failures near point loads is treated coarsely here and can be improved upon.

As shown in Fig. 14, the analysis using 54 elements and the tension stiffening relationships in Eq. (21) of the Appendix produce

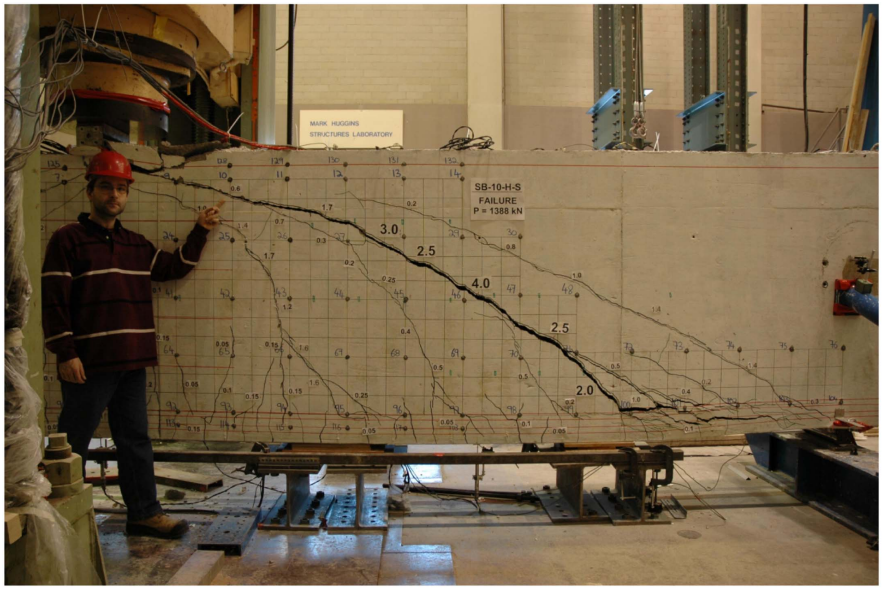

(a)

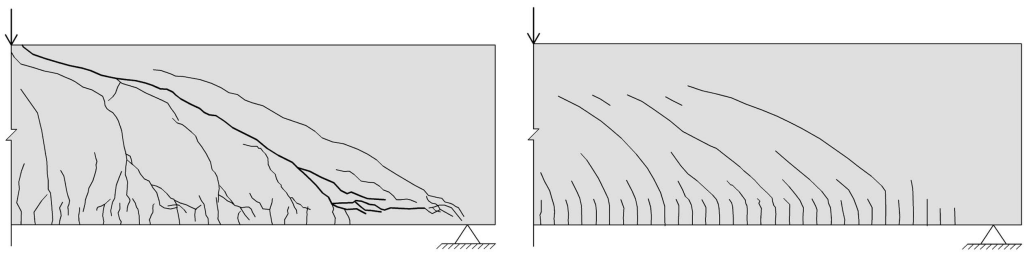

(b) (c)

Fig. 13. Crack patterns of L-10HS at failure: (a) Sherwood standing beside tested specimen; (b) observed crack pattern; and (c) crack pattern from finite-element analysis using proposed method.

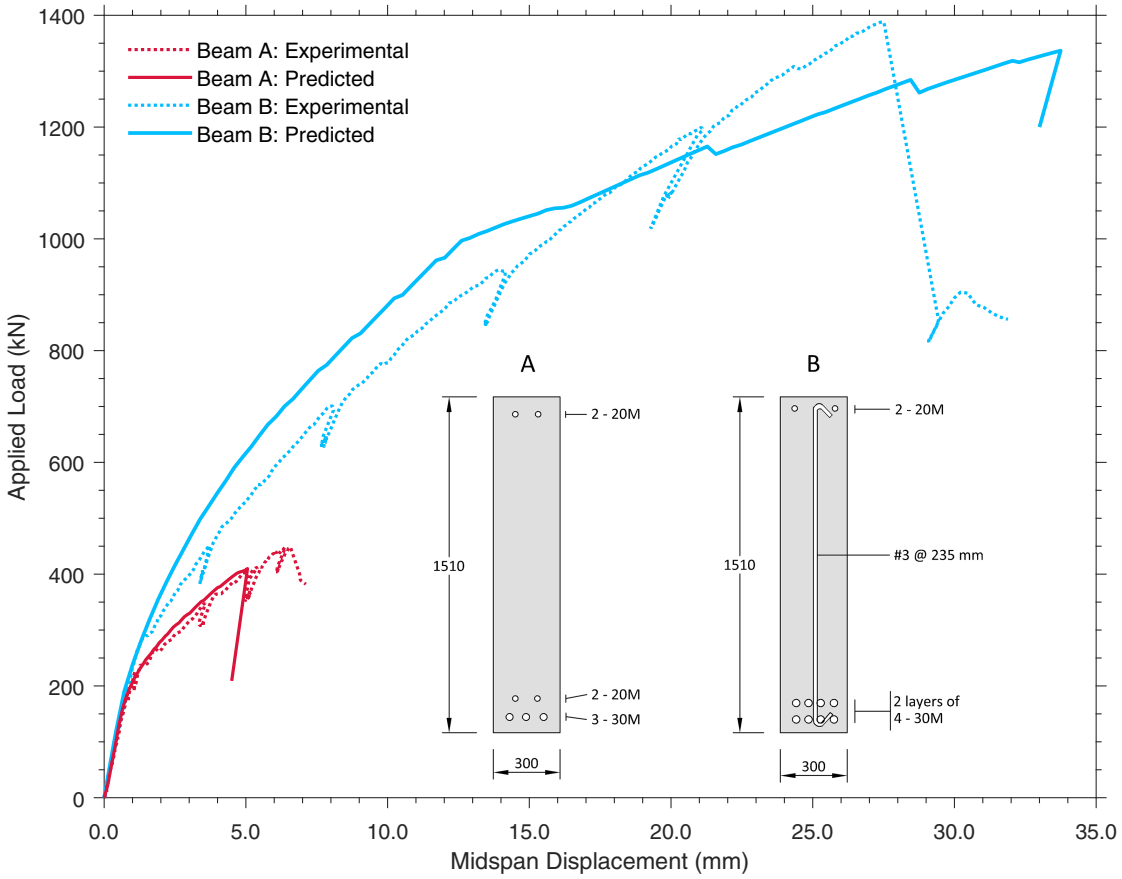

Fig. 14. Observed and modeled shear failures for beam with (L-10HS) and without (L-10HS) stirrups.

excellent estimates of the load-deformation behavior of these two large tests. Both members were predicted to fail in shear and at appropriate estimates of the experimental force and deformation. Fig. 13 shows the predicted and observed crack patterns. Here the calculated angle, θ, from the MCFT was used at middepth and a linear variation in angle was used elsewhere, reaching zero at the flexural compression face. The figure shows this to be a good approximation for the purpose of presenting crack diagrams for shear tests.

Close inspection of the prediction in Fig. 14 for the member with stirrups shows locations where the force prediction dropped to a slightly lower force as loading continued. These occurred because new elements along the length of the mesh were predicted to crack diagonally, which lowers the stiffness of the member as a whole. This, along with the ability to model nonconstant moments, is one of the key reasons that multiple elements along length of the member are needed. The decrease in predicted displacement after failure is artificial and is due to localization of damage within a single element.

To explore how many elements are required for good results, the mesh sensitivity analysis in Fig. 15 was conducted for Member L-10HS. With these analyses, the regions of the beam extending beyond the supports in the tested specimens were neglected [meshes in Fig. 15(a) show examples of this], and the K_v terms in the stiffness matrix for elements adjacent to point loads were made 1,000 times stiffer than as calculated in Eq. (7) in Section 4. The latter change was required because when elements get very short longitudinally, they demonstrate an unrealistic amount of predicted support settlement (i.e., transverse deformation) due to the concentrated loading or reaction forces. As mentioned previously, elements occurring within $d = 1{,}400$ mm from the central point load were given higher shear strength to suppress shear failures there [darker shade in Fig. 15(a)].

Fig. 15(b) shows the calculation of elastic flexural stiffness as the number of elements is increased. The beam theory line includes elastic shear deformations because the model includes these as well. Although the model converged to the theoretical solution with code-estimated concrete stiffness and uncracked transformed moment of inertia, it did not converge to the test result. This is a reminder of the challenges of modeling the behavior of concrete, even when uncracked. From Fig. 14, however, for engineering purposes, the uncracked stiffness was modeled sufficiently well even with a relatively small number of elements.

Fig. 15(c) shows the sensitivity in predicted shear strength with the number of elements in the analysis showing a relatively low sensitivity and that the results converged approximately to the experimental result. The lack of a smooth predicted change in failure load as the number of elements increased demonstrates the relatively complex interaction of bottom flange cracking and shear cracking as the mesh density goes up. Fig. 15(d) shows that the predicted deformation at maximum predicted load also converged but more slowly than did the shear strength. It might be surprising that an analysis with an insufficient number of elements overestimated deformations at ultimate limits states; when elements are too large, the member shear deformations are overestimated because high shear strains are applied over an inappropriately longer length than with smaller elements. The meshing strategy was to aim for all elements to be about the same length subject to the limitation of the fixed boundary line location between the stronger and weaker areas.

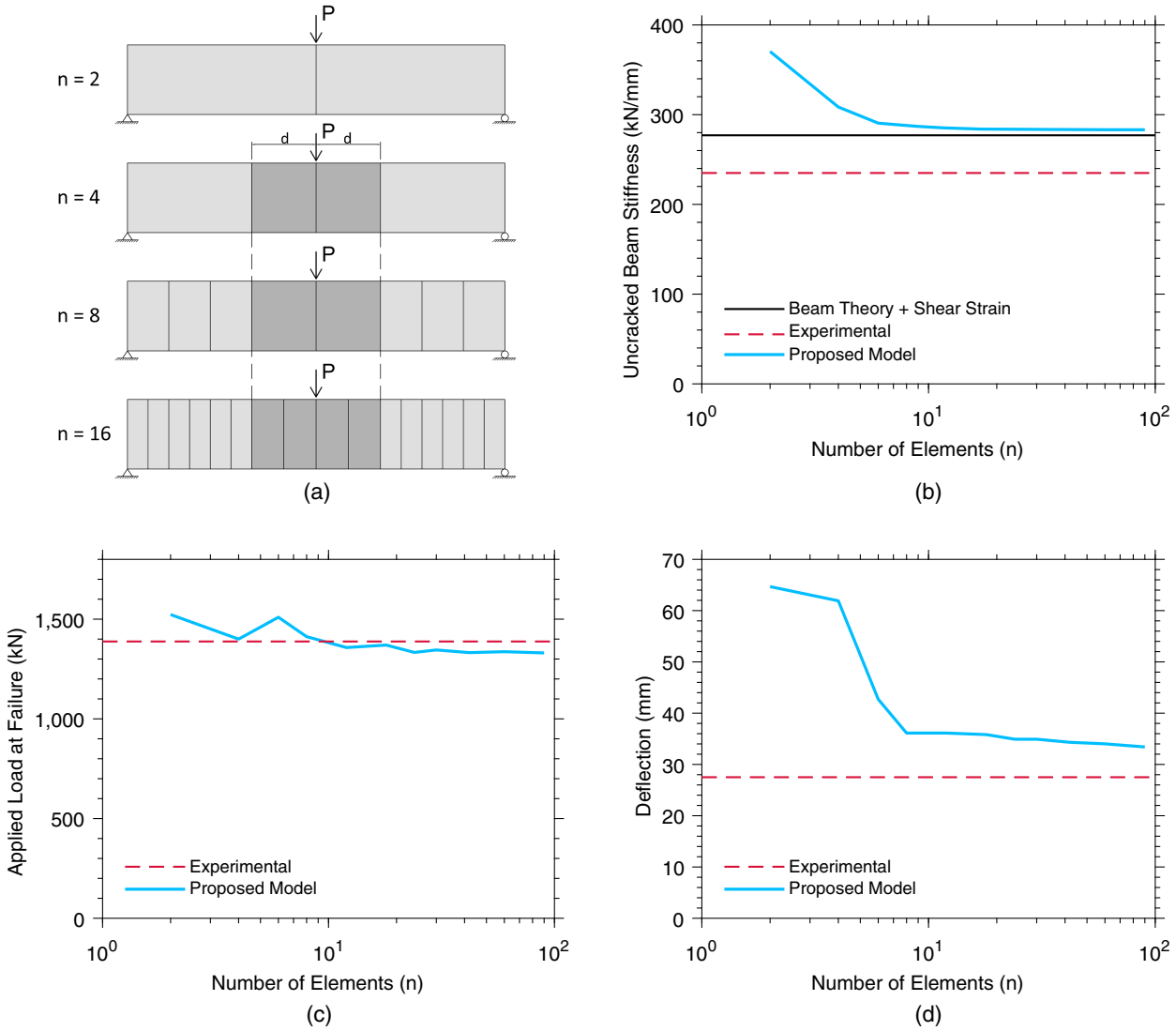

Fig. 15. Mesh sensitivity analysis using proposed element against results of Test L-10HS: (a) element mesh; (b) uncracked elastic stiffness; (c) shear strength; and (d) deflection.

Overall, the results from Fig. 15 indicate that elements should be at least half a member depth in length, $h/2$, but need not be made much shorter than a quarter, $h/4$, to get good results for strength and stiffness.

Shear-Critical Slender Beam Database

Structural analysis models using the proposed element were built to replicate individual reinforced concrete beam tests found in the largest publicly available database for shear-critical experimental results compiled by the American Concrete Institute (Reineck et al. 2013, 2014). The predicted failure load from an analysis was compared with the recorded experimental failure load [denoted as the experimental/predicted (Exp./Pred.) ratio]. A ratio greater than 1.0 implied that the analysis was conservative and underpredicted the actual failure load, which in theory is an acceptable outcome from a design perspective because the safety of the structure is guaranteed. The analysis results using the proposed element are illustrated in Fig. 16(a). These conservative results are especially important in shear-critical cases because the failure mechanism of such structures is brittle and occurs without much warning.

Table 1 summarizes the results of the FEM analysis using the proposed element and compares them with results using three other design codes taken from Mari et al. (2016). The results from this validation exercise (Bruun 2017) have been broken down into beams with and without stirrups and whether the beam had a rectangular or T-shaped cross section. As seen in Figs. 16(b and c), good agreement with the cumulative density function of a normal distribution was shown for the lower half of the results for both cases. This implies that there was no systematic error in the use of the proposed element in predicting beams that fell into the lower unsafe range. The results for the 782 beams without stirrups are best represented with a normal distribution $(\text{Exp./Pred.}) \sim N(1.308, 0.206^2)$, with a coefficient of variation (COV) of 15.8% and a fifth percentile value of 0.96 (i.e., 5% of tests fell below this value). The results for the 167 beams with stirrups are best represented with a normal distribution, $(\text{Exp./Pred.}) \sim N(1.40, 0.294^2)$, with a coefficient of variation of 21.0% and a fifth percentile value of 0.92. These values are improvements to the statistical results obtained from the analyses based on the ACI 318-11 (ACI 2011) and EC-2 (BSI 2008) design codes in Table 1 (CSA 2014).

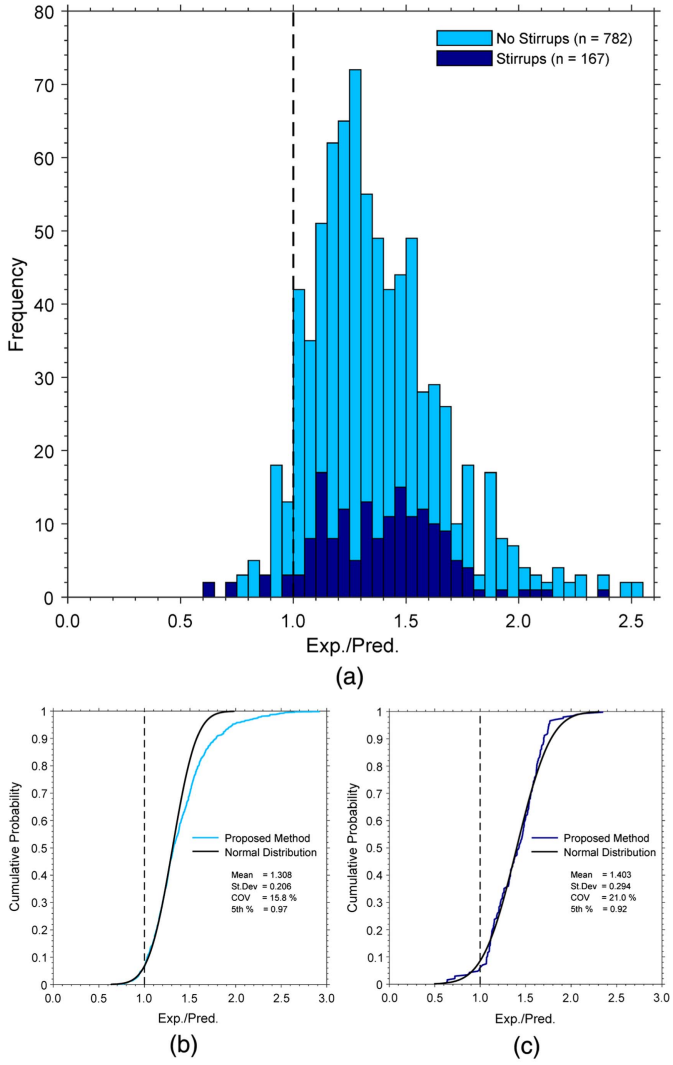

Fig. 16. Analysis results for full shear-critical beam test database: (a) histogram of analysis results; CDFs assuming a normal distribution for (b) no stirrups; and (c) stirrups.

Conclusion

This paper derived and validated a novel finite element for reinforced concrete that can be used to accurately analyze shear-critical beams and columns. The element was specifically formulated to span the full depth of a cross section, using only eight translational DOFs (two per node) to calculate the strain state and then represent the complex behavior typical of reinforced concrete. The stiffness matrix for the element was assembled from three separate components:

- K_1 (flexure/axial): based on the axial strain distribution calculated at the top and bottom of the cross section;
- K_2 (shear): based on shear strain and longitudinal strain at middepth calculated from the nodal displacements. A MCFT analysis was performed to determine the transverse strain associated with a zero clamping stress condition. The resulting shear stiffness generates K_2; and
- K_3 (diagonal cracking): based on the angle of diagonal cracking, θ, calculated from the MCFT analysis, this captures the additional demand on the longitudinal reinforcement due to shear after diagonal cracking.

Individual simply supported beams can be accurately modeled to find the shear strength with just 10–20 elements along the length of the member. An element length between $1/2$ and $1/4$ the depth of the member is generally recommended for this type of analysis. In general, a finite-element analysis using the proposed element was shown to require significantly fewer degrees of freedom than an analysis using traditional 2D elements to produce accurate results.

The full validation of the element was performed against the experimental results from a database of shear-critical reinforced concrete beams: 782 beams without shear reinforcement and 167 beams with shear reinforcement were modeled. The results from the FEM analyses using the proposed element showed improvements compared with the results when using ACI 318-11 (ACI 2011) and EC-2 (BSI 2008) design codes. Future development of the element will focus on expanding the types of loading conditions, structures (e.g., concrete frames and frames with walls), and failure modes that can be accurately modeled.

Appendix. Modified Tension-Stiffening Relationship

In generating Fig. 11, the constitutive equations in Fig. 2 could have been used and would produce reasonable results for this case. However, the results for other members, such as those without stirrups, are relatively sensitive to the assumed tension-stiffening relationship. It is thus recommended that the tension stiffening relationship in Fig. 2, be replaced with an alternate. For shear analyses at depths of a beam that are within 15 bar diameters of concentrated longitudinal reinforcement, the Bentz (2005) model should be used. When depths of interest are further from longitudinal reinforcing steel, the tension stiffening (f_1) is less governed by the principal tensile strain (ε_1) but by shear on the crack (v_{ci}) instead. For such cases, it is recommended that, after diagonal cracking, the tension-stiffening relationship instead be taken as follows:

$$f_1 = \min\left(\frac{v_{ci}}{\tan(\theta)}, v_{ci} \cdot \tan(\theta)\right)$$
$$v_{ci} = \frac{v_{ci,\max}}{2} \tag{21}$$

Table 1. Shear test database summary (based on 2013 version of database)

	No stirrups				Stirrups			
Type	n	μ	COV (%)	5th percentile	n	μ	COV (%)	5th percentile
ACI 318-11	784	1.42	38.3	—	170	1.52	22.3	—
EC-2	784	1.10	27.9	—	170	1.44	17.9	—
CSA A23.3-14	784	1.22	22.3	—	170	1.29	29.8	—
Proposed element	782	1.30	15.8	0.96	167	1.40	21.0	0.92
Rectangular beam	718	1.30	15.2	0.97	113	1.33	16.6	0.96
T-beam	64	1.51	16.6	1.10	54	1.53	26.2	0.87

where $v_{ci,\max}$ = maximum value of Eq. (15) in Fig. 2. This proposed equation uses only 50% of the MCFT maximum shear on the crack because the implementation already includes tension stiffening, unlike design codes based on the MCFT. This maximum shear on the crack is a function of concrete strength, aggregate size, and the calculated crack width, w. In determining this crack width, the longitudinal direction crack spacing, s_x, should be taken as the shear depth, $d_v = 0.9d$, and in the transverse direction, the crack spacing, s_z, should be taken as 300 mm if minimum stirrups are provided or five times the member depth otherwise. For concrete strengths in excess of 70 MPa, the aggregate size, a_g, should be taken as zero because cracks tend to cleave the aggregate rather than form around them. Also, when a shear crack exceeds 25 mm, the stirrups are assumed to rupture and thus can no longer resist any force. Some of the very conservative predictions in Fig. 16(a) may indicate that the experiment showed strut-and-tie behavior, which the proposed method in this paper cannot account for well.

Data Availability Statement

Some or all data, models, or code that support the findings of this study are available from the corresponding author upon reasonable request.

Acknowledgments

The authors would like to acknowledge the support of the Natural Sciences and Engineering Research Council (NSERC) of Canada.

Notation

The following symbols are used in this paper:

A_c, A_s = area of concrete and steel;
a = maximum size of coarse aggregate;
b = width of cross section at given depth;
b_w = minimum web width of cross section;
d = distance from extreme compression fiber to centroid of tension reinforcement;
d_c, d_s = depth of concrete and steel;
d_v = shear depth;
d_x = longitudinal length of an element;
$d\varepsilon_{\text{top}}$, $d\varepsilon_{\text{bot}}$ = incremental strain at top and bottom of the element;
$\bar{E}_c$, $\bar{E}_s$ = longitudinal secant stiffness for concrete and steel;
$\bar{E}_{c1}$, $\bar{E}_{c2}$ = principal tension and compression secant stiffness;
F = force acting on the effective shear panel area;
F_t, F_b = horizontal force in top and bottom of element;
F_x = additional cracking tensile force [Eq. (17)];
F_x, F_y = applied horizontal and vertical shear force at node [Fig. 7(b)];
f_{cr} = tensile strength of concrete;
f_{cx} = longitudinal component of shear stresses carried by diagonally cracked concrete;
f_{sx}, f_{sy} = average stress in steel reinforcement in x- and y-directions;
f_{sxcr}, f_{sycr} = local stress in reinforcement at the crack in the x and y direction;
f_x, f_y = stress in the x- and y-directions;
$f_{x,\text{yield}}$, $f_{y,\text{yield}}$ = yield stress in the x- and y-direction steel;
$\bar{G}$ = shear secant stiffness;
h = overall depth of cross section;
K_B, K_T, K_{TB}, K_{BT} = flexure/axial matrix longitudinal stiffness terms;
K_v = flexure/axial matrix vertical stiffness terms;
K_1, K_2, K_3 = flexure/axial, shear, and diagonal cracking stiffness matrices;
k_s = stiffness of stirrup steel;
M_T, M_B = moment about top or bottom of cross section;
N, M, V = axial, moment, and shear forces on cross section;
s_x, s_y = crack spacing in the x- and y-directions;
s_θ = diagonal crack spacing;
u = unit displacement;
v = shear stress (MCFT);
v_{ci} = shear stresses on crack face resisted by aggregate interlock;
$v_{ci,\max}$ = maximum shear stresses on crack face resisted by aggregate interlock;
w = crack width;
y = vertical distance measured from the bottom of the cross section;
ΔF_x = change in horizontal force at node;
Δ_x, Δ_y = horizontal and vertical displacement of node;
ε_c, f_c = concrete strain and stress;
ε'_c, f'_c = concrete strain and stress at maximum capacity of cylinder;
ε_s, f_s = steel strain and stress;
ε_{top}, ε_{bot} = average longitudinal strain at the top and bottom of the element;
ε_x, f_x = longitudinal strain and stress;
ε_y, f_y = transverse strain and stress;
ε_1, f_1 = average principal tensile strain and stress;
ε_2, f_2 = average principal compressive strain and stress;
ϕ = curvature due to moment;
γ_{xy}, v_{xy} = shear strain and stress;
μ = mean of normal distribution;
ρ_x, ρ_y = percentage reinforcement in x- and y-directions of shear panel;
θ = angle of principal compressive stresses to the longitudinal axis of the member; and
θ_L = rigid-body rotation angle (left side).

References

AASHTO. 2020. *LRFD bridge design specifications and commentary*. 9th ed. Washington, DC: AASHTO.

Acevedo, A. B., E. C. Bentz, and M. P. Collins. 2009. "Influence of clamping stresses in the shear strength of concrete slabs under uniform loads." Supplement, *J. Earthquake Eng.* 13 (S1): 1–17. https://doi.org/10.1080/13632460902813190.

ACI (American Concrete Institute). 1963. *Building code requirements for structural concrete*. ACI 318-63. Farmington Hills, MI: ACI.

ACI (American Concrete Institute). 2011. *Building code requirements for structural concrete*. ACI 318-11. Farmington Hills, MI: ACI.

ACI (American Concrete Institute). 2019. *Building code requirements for structural concrete*. ACI 318-19. Farmington Hills, MI: ACI.

Adeghe, L. 1986. “A finite element model for studying reinforced concrete detailing problems.” Ph.D. thesis, Dept. of Civil Engineering, Univ. of Toronto.

Bathe, K.-J. 2014. *Finite element procedures*. 2nd ed. Englewood Cliffs, NJ: Prentice-Hall.

Bentz, E. C. 2000a. “Response-2000.” Accessed May 31, 2022. https://www.hadrianworks.com/.

Bentz, E. C. 2000b. “Sectional analysis of reinforced concrete members.” Ph.D. thesis, Dept. of Civil Engineering, Univ. of Toronto.

Bentz, E. C. 2005. “Explaining the riddle of tension stiffening models for shear panel experiments.” *J. Struct. Eng.* 131 (9): 1422–1425. https://doi.org/10.1061/(ASCE)0733-9445(2005)131:9(1422).

Birely, A. C., L. N. Lowes, and D. E. Lehman. 2012. “Linear analysis of concrete frames considering joint flexibility.” *ACI Struct. J.* 109 (3): 381–392.

Bruun, E. P. G. 2017. “The hybrid panel-truss element: Developing a novel finite element for the nonlinear analysis of reinforced concrete beams and shells.” M.S. thesis, Dept. of Civil and Mineral Engineering, Univ. of Toronto. https://tspace.library.utoronto.ca/handle/1807/79117.

BSI (British Standard Institution). 2008. *Design of concrete structures*. Eurocode 2 (EC-2). London: BSI.

Collins, M. P., E. C. Bentz, P. T. Quach, and G. T. Proestos. 2015. “The challenge of predicting the shear strength of very thick slabs.” *Concr. Int.* 37 (11): 29–37.

Collins, M. P., and D. Mitchell. 1997. *Prestressed concrete structures*. Toronto: Response Publications.

Cross, H. 1930. “Analysis of continuous frames by distributing fixed-end moments.” *Proc. Am. Soc. Civ. Eng.* 96 (1): 1–10. https://doi.org/10.1061/TACEAT.0004333.

CSA (Canadian Standards Association). 2014. *Design of concrete structures*. CSA A23.3-14. Ottawa: CSA.

CSA (Canadian Standards Association). 2019. *Design of concrete structures—Clause 11—Shear and torsion*. CSA A23.3-14. Ottawa: CSA.

Jouravski, D. 1856. “Remarques sur la résistance d’un corps prismatique et d’une pièce composée en bois ou en tôle de fer a une force perpendiculaire à leur longueur.” *Ann. Ponts Chaussées* 12: 328–351.

Kaufmann, W., and P. Marti. 1998. “Structural concrete: Cracked membrane model.” *J. Struct. Eng.* 124 (12): 1467–1475. https://doi.org/10.1061/(ASCE)0733-9445(1998)124:12(1467).

Maekawa, K., H. Okamura, and A. Pimanmas. 2003. *Non-linear mechanics of reinforced concrete*. London: CRC Press.

Mari, A., J. M. Bairam, A. Cladera, and E. Oller. 2016. “Shear design and assessment of reinforced and prestressed concrete beams based on a mechanical model.” *J. Struct. Eng.* 142 (10): 04016064. https://doi.org/10.1061/(ASCE)ST.1943-541X.0001539.

Mitchell, D., and M. P. Collins. 1974. “Diagonal compression field theory—A rational model for structural concrete in pure torsion.” *ACI J.* 71 (8): 396–408. https://doi.org/10.14359/7103.

Reineck, K.-H., E. C. Bentz, B. Fitik, D. A. Kuchma, and O. Bayrak. 2013. “ACI-DAfStb database of shear tests on slender reinforced concrete beams without stirrups.” *ACI Struct. J.* 110 (5): 867–876. https://doi.org/10.14359/51685839.

Reineck, K.-H., E. C. Bentz, B. Fitik, D. A. Kuchma, and O. Bayrak. 2014. “ACI-DAfStb databases for shear tests on slender reinforced concrete beams with stirrups.” *ACI Struct. J.* 111 (5): 1147–1156. https://doi.org/10.14359/51686819.

Sherwood, E. G. 2008. “One-way shear behaviour of large, lightly-reinforced concrete beams and slabs.” Ph.D. thesis, Dept. of Civil Engineering, Univ. of Toronto.

Sherwood, E. G., E. C. Bentz, and M. P. Collins. 2007. “Effect of aggregate size on beam-shear strength of thick slabs.” *ACI Struct. J.* 104 (2): 180–190. https://doi.org/10.14359/18530.

Stevens, N. 1987. “Analytical modelling of reinforced concrete subjected to monotonic and reversed loadings.” Ph.D. thesis, Dept. of Civil Engineering, Univ. of Toronto.

Turneaure, F. E. 1908. *Cyclopedia of Civil Engineering: A general reference work on surveying, railroad engineering, structural engineering, roofs and bridges, masonry and reinforced concrete, highway construction, hydraulic engineering, irrigation, river and harbor improvement, municipal engineering, cost analysis, etc*. Chicago: American School of Correspondence.

Uzel, A. 2003. “Shear design of large footings.” Ph.D. thesis, Dept. of Civil Engineering, Univ. of Toronto.

Vecchio, F. J. 1989. “Nonlinear finite element analysis of reinforced concrete membranes.” *ACI Struct. J.* 86 (1): 26–35. https://doi.org/10.14359/2620.

Vecchio, F. J. 1990. “Reinforced concrete membrane element formulations.” *J. Struct. Eng.* 116 (3): 730–750. https://doi.org/10.1061/(ASCE)0733-9445(1990)116:3(730).

Vecchio, F. J. 2001. “Non-linear finite element analysis of reinforced concrete: At the crossroads?” *Struct. Concr.* 2 (4): 201–212. https://doi.org/10.1680/stco.2001.2.4.201.

Vecchio, F. J., and M. P. Collins. 1986. “The modified compression-field theory for reinforced concrete elements subjected to shear.” *ACI J.* 83 (2): 219–231. https://doi.org/10.14359/10416.

Vecchio, F. J., D. Lai, W. Shim, and J. Ng. 2001. “Disturbed stress field model for reinforced concrete: Validation.” *J. Struct. Eng.* 127 (4): 350–358. https://doi.org/10.1061/(ASCE)0733-9445(2001)127:4(350).